# LANGMUIR

pubs.acs.org/Langmuir Article

# Crystal Comets: A Geometric Model for Sculpting Anisotropic Particles from Emulsions

Mathew Q. Giso, Haoda Zhao, Patrick T. Spicer, and Timothy J. Atherton\*



Cite This: https://dx.doi.org/10.1021/acs.langmuir.0c02249



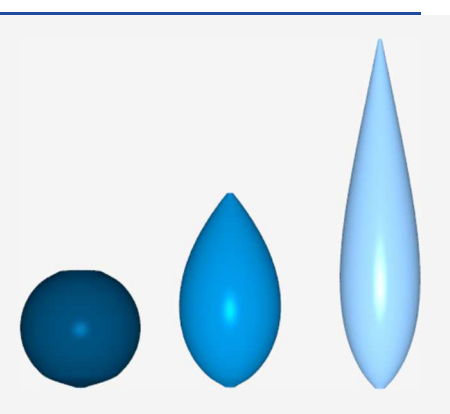
**ACCESS** 

Metrics & More

Article Recommendations

Supporting Information

ABSTRACT: Microscopic high aspect ratio particles have many applications including enhanced delivery of active ingredients and food stability. Here, we develop a simple, scalable process that produces particles with a continuously controllable aspect ratio. Oil-in-water emulsion droplets are quenched and crystallize in the presence of surfactants that facilitate the ejection of the solid oil phase from its liquid precursor. Tuning the ejection and crystallization rates to be comparable, by adjusting the surfactant concentration and quench depth, promotes anisotropic particle growth by continuously ejecting solidified oil from the precursor droplet as the crystallization proceeds. We predict the accessible morphologies using an analytical geometric model that indicates a nonconstant contact angle during the crystallization process. We see that the crystal aspect ratio is dependent on the surfactant concentration, which can be explained as a variation of the maximum growth angle achieved during crystallization.



#### **■ INTRODUCTION**

Emulsions are mixtures of immiscible fluids that phase separate into small droplets dispersed in a continuous fluid phase. They are commercially important for food products,  $^{1,2}$  purification, and encapsulation of therapeutics. Emulsion droplets can change their morphology when cooled. If an emulsion is cooled below the freezing point of the droplets,  $T_{\rm d}$ , but above that of the continuous phase,  $T_{\rm h}$ , where we assume  $T_{\rm d} > T_{\rm h}$ , then the droplets will begin to solidify. This is a common technique to build a structure in dairy emulsions. Crystals cause bridges to form between droplets and induce flocculation. Typically, the growing solid phase is preferentially wetted by its liquid phase. This behavior can be modified by the addition of surfactants, causing the growing crystals to be ejected from their own melt.  $^{8,11-13}$ 

Careful tuning of the surfactant concentration can be used to control the rate of ejection, while the rate of crystallization can be modified by how quickly the system is cooled. As these rates become comparable, the growing crystal is continuously ejected from the precursor droplet as it grows. In this regime, the resulting crystals, dubbed "comets", become highly elongated. This process is an attractive means to create anisotropic microscopic particles because it is highly scalable, resulting from a bulk phase transition, and is readily controllable by macroscopic parameters.

Sculpting large numbers of anisotropic microscopic particles is of great interest to the medical and food industries. High aspect ratio particles have been shown to remain in the circulatory system longer than spherical ones<sup>14</sup> and can improve drug delivery to lower airway regions via inhalers. <sup>15,16</sup> Elongated particles have also been shown to help with the

stability of foods,  $^{17,18}$  likely due to improved packing efficiency.  $^{19}$ 

For all of these applications, tuning the crystal morphology is of crucial importance. In this paper, we aim to develop a systematic understanding of how the highly nonequilibrium growth process impacts the crystal morphology. We use these insights to predict how the size and shape of the sculpted particles depend on the experimental control parameters. Specifically, we will vary the surfactant concentration while holding the crystallization rate constant. To do so, we develop in the Model section a semianalytical geometric model based on Anderson et al.'s model of the crystallization of a sessile droplet.<sup>20</sup> Our model incorporates dynamic boundaries and a finite precursor reservoir. Models of solidification with dynamic boundaries are relevant in a wide range of crystallization processes, <sup>21–23</sup> including the production of silicon wafers.<sup>24</sup> We test these predictions experimentally in the Results and Discussion section before concluding.

# SYSTEM

The experimental system under consideration is shown in Figure 1A. A fluid lipid droplet is surrounded by an aqueous host. The system is then cooled and the lipid begins to crystallize. If an appropriate level of surfactant is added to the

Received: July 30, 2020 Revised: October 16, 2020



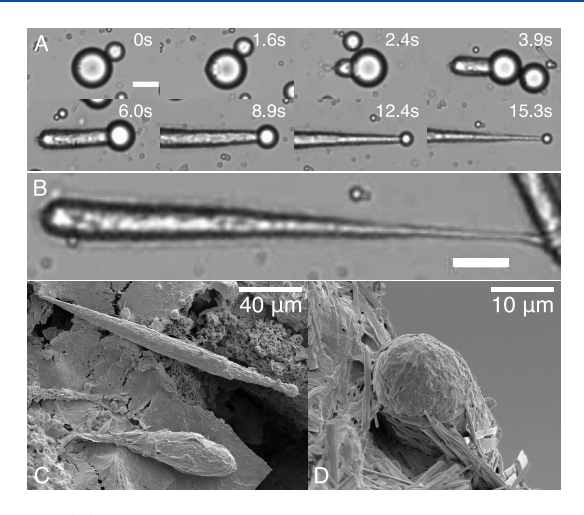


Figure 1. (A) Time sequence of a crystal formed in a 1.5 wt % sodium dodecyl sulfate (SDS)/decanol solution with a 1.2 °C/s cooling rate and (B) the resulting crystal. (C) Side and (D) end views of crystals formed at a 1.5 wt % SDS/decanol surfactant concentration. Scale bars are 20  $\mu$ m unless otherwise specified.

aqueous host, the liquid lipid phase can be induced to eject its own crystalline phase. <sup>11</sup> At t = 0 s, we have the initial fluid lipid droplet. At t = 1.6 s, a nucleation site appears and begins to grow until it is ejected. This process continues for another 13.7 s, with crystal growth constrained to the oil—crystal interface. The final solid particle shown in Figure 1B is tapered and has a high aspect ratio with a length more than  $10\times$  greater than the original droplet. The scanning electron microscopy (SEM) image in Figure 1C shows two crystals side by side in detail. These illustrate the range of accessible morphologies. Figure 1D shows an end view of a crystal displaying its axisymmetric profile.

The comet sculpting process begins with a small crystal growing within its precursor droplet. Once large enough, the growing crystal may, for example, pierce the edge of the droplet and be partially or completely ejected depending on the crystal's wettability. The ejection behavior causes the three-phase contact line to move as crystallization proceeds. The kinetics of crystallization can change the final resting place of a crystal formed at an interface. The contact angle that the crystal makes with the interface can be different from the contact angle predicted by the Young–Dupré equation. Crystallization cannot occur in regions no longer in contact with the liquid lipid phase. As the initial fluid droplet is depleted, the crystals begin to taper, enabling the production of anisotropic morphologies lacking mirror symmetry between the head and the tail.

Experimentally, ejection is controlled by adjusting the surfactant concentration to modify the wettability of the oil crystals. Generally, this process is slow to occur, taking hours for complete ejection of the crystals. A cosurfactant can be added to accelerate ejection by changing the surfactant packing efficiency at the liquid lipid—water interface. Previous work by Spicer and Hartel shows that faster cooling rates usually produce more elongated shapes than slow cooling rates by allowing the crystallization to keep pace with the rate of ejection.

To predict the shape of the crystals, we will develop a model inspired by crystallization processes with moving contact lines in containerless solidification.<sup>20</sup> It is purely geometric and aims to predict the qualitative features of the crystal shape. The

model is a simplified scenario and neglects temperature gradients and fluid flow.

#### MODEL

The geometry that we consider consists of a crystal component, a fluid precursor, and a background host fluid as shown in Figure 2. The model assumes that the crystals are

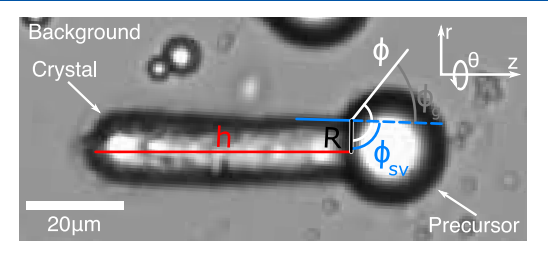


Figure 2. Schematic of the geometric model with relevant components labeled.

axisymmetric and that the crystal—precursor interface, or solidification front, remains flat as growth proceeds. This is consistent with a model of one-dimensional (1D) heat conduction. In cylindrical coordinates, the height of the crystal, h, is the distance from the start of the crystal to the solidification front. In the radial direction, R is the radius of the solidification front. The three-phase contact line forms a circle at the edge of the crystal—precursor interface and can be given parametrically in cylindrical coordinates by

$$X = (R(h), \theta, h) \tag{1}$$

where  $\theta \in [0,2\pi]$  because the system is axisymmetric. The contact angle (colored white in Figure 2),  $\phi(t)$ , is the angle between the precursor—background tangent at the three-phase contact line and the solidification front. The angle  $\phi_{\rm SV}$  (colored blue in Figure 2) is defined between the solid—background tangent at the three-phase contact line and the solidification front. The three-phase contact line moves as the fluid precursor is converted into solid. Evaluating the volume of precursor that crystallizes in a cylindrically symmetric volume of height  $\mathrm{d}h$  and accounting for the density change yields

$$\frac{\mathrm{d}V}{\mathrm{d}h} = -\pi\rho R^2 \tag{2}$$

where  $\rho = \rho_{\rm s}/\rho_{\rm l}$  is the density ratio between the solid and fluid phases, respectively. Assuming that the fluid droplet remains spherical, the instantaneous volume of the droplet is calculated from the spherical cap defined by R and  $\phi$ 

$$V = \frac{2\pi}{3} \frac{R^3 (1 - \cos\phi)^2 \left(1 + \frac{1}{2}\cos\phi\right)}{\sin^3\phi}$$
 (3)

Typically, the crystal does not grow tangentially to the precursor—background interface but lies at some angle to it. This angle is known as the growth angle,  $\phi_{\rm g}$ . It measures the angle between  $\phi$  and  $\phi_{\rm SV}$  and is colored gray in Figure 2. A trijunction condition is required to relate  $\phi_{\rm g}$  to R and h

$$\frac{\mathrm{d}R}{\mathrm{d}h} = -1/\tan(\phi - \phi_{\mathrm{g}}) \tag{4}$$

This relation can be found by allowing growth in the direction of the solid-background tangent. The change in radius and

height can then be related using tangent. The shape of the final droplet is then determined by the initial conditions  $R_0$ ,  $\phi_0$ , and parameters  $\rho$  and  $\phi_g$ . The system of eqs 2–4 can then be integrated numerically.

Growth proceeds from an initially small seed where the precursor droplet is initially spherical. This corresponds to  $\phi_0 \sim \pi$  and a small value for  $R_0$ . The initial volume of the precursor droplet  $V_0$  is fixed. Initially, we assume that  $\phi_{\rm g}$  is constant. The contact angle as a function of position and corresponding shapes as a function of  $\phi_{\rm g}$  are shown in Figure 3A. These trends are nondimensionalized by dividing by  $V_0^{1/3}$ .

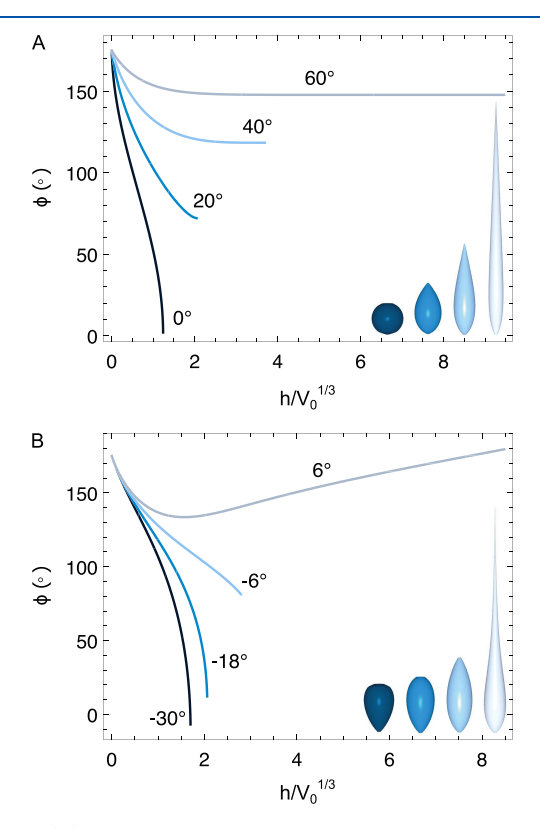


Figure 3. (A) Crystals grown using a constant growth angle with an initial contact angle of 175°. (B) Crystals grown using different values of  $\phi'_g$  with  $\phi_0 = 175^\circ$  and an initial growth angle of 50°. All crystals were grown with an initial volume of unity and a  $\rho = 1.1$ .

The predicted shapes resemble the experimental observations in Figure 1. The contours widen from the initial seed and then narrow as the precursor droplet is depleted. If  $\phi_{\rm g}=0$ , the direction of growth coincides with the precursor–background interface at all times, resulting in a circular particle. As  $\phi_{\rm g}$  increases, so do the length and aspect ratio of the crystals. For

large  $\phi_g$ , growth culminates in a regime where the contact angle approaches a constant value, resulting in a nearly conical tail as discussed in Anderson et al.'s work. An important property of these crystals is their constant concavity. All of the crystals formed at a constant growth angle have a concave down profile, that is, R''(h) < 0. As  $\phi(h)$  and R(h) are coupled by eq 4, a decreasing  $\phi(h)$  implies that the interface is growing smaller. Also visible are inflection points in the curve for  $\phi_g = 0^\circ$ . This occurs when the sum  $\phi(h) - \phi_g$  in eq 4 crosses  $\pi/2$ .

Experimentally, crystals are often observed with a change in concavity. This can be achieved in the geometric model by allowing  $\phi_{\rm g}$  to vary. We allow it to change with a constant slope  $\frac{{\rm d}\phi_{\rm g}}{{\rm d}h}=\phi_{\rm g}'$  from an initial value of  $\phi_{\rm g0}=50^\circ$ . We show the resulting shapes in Figure 3B. A decreasing growth angle tends to attenuate and widen the tail, while an increasing growth angle causes a change in the concavity of the tail. This behavior is indicated by an increasing contact angle at the late stages of growth.

Using these results, we can explain the formation of a wide range of crystal morphologies through variations in  $\phi_{e0}$ ,  $\phi'_{e'}$  and  $\rho$ . The phase diagram in Figure 4 shows the outlines of the accessible morphologies. As we have shown, the length of the crystal increases monotonically with the initial growth angle, provided  $\phi_{\mathrm{g}}' \leq 0$ . Variation in the growth angle with height modifies the tail of the crystal. An increasing growth angle will induce a change in concavity, resulting in crystals with long and increasingly narrow tails. This too can modify the length of the crystal. A decreasing growth angle does the reverse; the contact angle approaches the precursor-crystal contact angle, which results in a more rounded head. As expected,  $\rho$  < 1 yields larger crystals due to the increase in volume. At high initial growth angle and slope, this density effect is small. This is due to the upper bound on the growth angle. In this region of the phase diagram, the entire precursor droplet is not converted into the crystal. Experimental evidence of crystals that do not use their entire precursor droplet will be discussed in subsequent sections.

#### **■ EXPERIMENTAL SECTION**

The system includes two lipids, trihydroxystearin (Peter Cremer, also known as castor wax) and stearic acid (95%, Sigma-Aldrich), with two surfactants to control dewetting phenomena, sodium dodecyl sulfate ( $\geq 99.0\%$ , Sigma-Aldrich) and decanol (98%, Sigma-Aldrich). Deionized water, made using a Milli-Q Advantage A10, was used to prepare all aqueous solutions.

Trihydroxystearin and stearic acid were combined at a ratio of 4:6, heated to 90 °C, and stirred well. The surfactant solution was prepared by dissolving sodium dodecyl sulfate (SDS) with cosurfactant decanol in Milli-Q water. Decanol was added at 10%

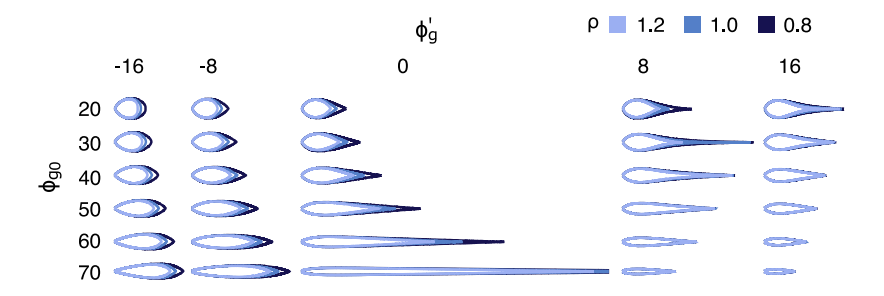
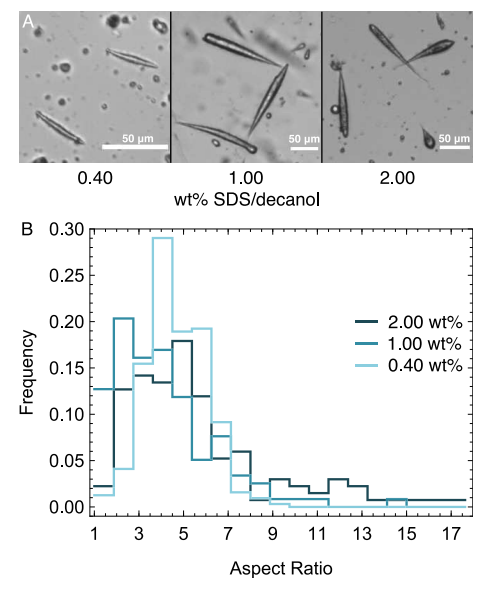


Figure 4. Phase diagram showing the crystals that result from a wide range of parameters. All crystals have an initial contact angle of  $175^{\circ}$  and a fixed initial volume. The color of each contour indicates its density ratio.

the weight of the SDS. The surfactant solution was heated to the same temperature as the melted lipid or lipid mixture and then the two systems combined and manually shaken to obtain a hot oil-in-water emulsion. A drop of the hot emulsion was then dropped by a pipette onto a glass slide and covered by a coverslip for observation of crystallization with an optical microscope as the system cooled to room temperature. To make elongated particles in bulk, 1 mL of the hot emulsion (90 °C) was added into a cooler surfactant solution. Holding the cold surfactant solutions at different temperatures allows control over the cooling rates, and hence the crystallization rate, imposed on the emulsion. The resulting crystals are shown in Figure SA.



**Figure 5.** (A) Table of representative crystals formed at different surfactant concentrations and a quench depth of 50 °C. This is the temperature difference between the surfactant solution and emulsion prior to mixing. (B) Histogram of crystal aspect ratios at different surfactant concentrations.

A Leica DM2500M was used to observe the lipid particles and micrographs were recorded using a Moticam 10 MP digital camera. High-speed videos were recorded using a QIMAGE optiMOS high-speed camera. ImageJ<sup>29</sup> was utilized to analyze the micrographs for particle size, shape, boxed aspect ratio, and contact angle, <sup>30,31</sup> between the oil droplets and crystal during their formation. The ImageJ reslice function was used to fit experimental crystal contours to contours predicted by the geometric model. These fits were used to obtain Figure 6 discussed below.

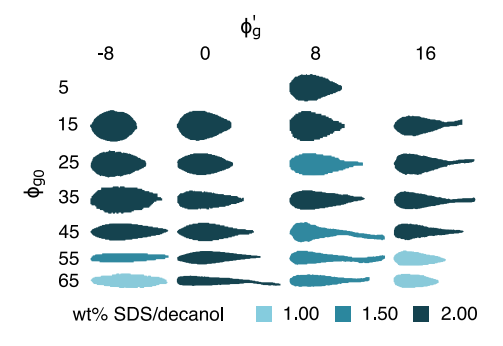


**Figure 6.** Thresholded images of crystals formed at various surfactant concentrations fit to  $\phi_{g0}$  and  $\phi'_g$  with  $\rho = 0.8$ . Images are not to scale.

#### RESULTS AND DISCUSSION

The initial emulsion contained droplets ranging in size from 10 to 40  $\mu$ m, with most droplets close to 10  $\mu$ m in size. The distributions of droplet size were similar across different surfactant concentrations (see the Supporting Information). The initial size of the droplet affects the final comet by setting the crystallizing mass available but did not strongly affect the resulting crystal shapes. Figure 5A maps the range of crystal morphologies obtained by systematically varying the concentration of surfactants and hence the crystal wettability. These crystals were generally between 40 and 5  $\mu$ m long and 5 and 75 um wide, with the occasional very large and long crystal. At low surfactant concentrations (not shown), spherical morphologies were seen exclusively. Increasing the surfactant concentration yields higher aspect ratio crystals by increasing the adsorption and dewetting rate. Histograms of crystal aspect ratios are shown in Figure 5B. The upper bound aspect ratio clearly increases with the surfactant concentration. Despite this, a large fraction of the crystals forms with lower aspect ratios.

Profiles of observed crystal morphologies are shown in Figure 6. The shapes observed are in the range of morphologies predicted in Figure 4. This suggests a spectrum of three-phase contact conditions at the same surfactant concentration. When  $\phi_{\mathrm{g0}}$  is low and  $\phi_{\mathrm{g}}'$  is low, we see broader heads consistent with a small initial growth angle. When  $\phi_{\mathrm{g0}}$  is high or  $\phi'_{g}$  is high, there is evidence of changes in concavity and long narrow tails that suggest an increasing growth angle. At median values of  $\phi_{g0}$  and small  $\phi_{g}'$  we see crystals that form with a straight edge. This indicates a nearly constant growth angle. There are smooth transitions between different morphologies, which agrees with the geometric model. Note also the variation in size in Figure 5 as some of these crystals do not use up their entire precursor droplet. Some morphologies seen in the geometric model did not appear in the experiment, particularly those with a low  $\phi_{\rm g0}$ . In general, the crystals seen in the experiment were asymmetric. This is due to droplets colliding with either other droplets or the substrate during crystallization. In addition, nonuniform surfactant adsorption can induce Marangoni flow, which has been shown to induce motion. 33,34 The wide range of behaviors indicates a nonconstant contact angle.

We measure the contact angle defined in Figure 2 for crystals formed at 2.00 wt % in Figure 7. The trends generally showed an initially decreasing contact angle with time. We

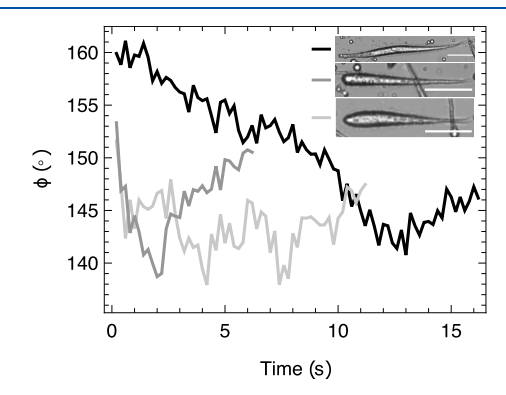


**Figure 7.** Contact angle between the oil droplet and crystal as a function of time for different crystals formed at 2.00 wt % SDS/decanol. Scale bars are 50  $\mu$ m.

would expect this decrease as the droplets are initially spherical  $(\phi \sim \pi)$  before ejection, which causes  $\phi$  to decrease. Some series showed a slight increase toward the end of the growth. This would suggest a change in concavity. Given the variation in the crystals that we see in Figure 6, variations in the contact angle trends are expected. Note that not all of the crystals form at the same rate. We would expect this to be dependent on the size of the droplets to some degree, but the crystals with a lower surfactant concentration formed more quickly than their high-surfactant counterparts.

Our combined theoretical and experimental study produces the following picture of how the growth process impacts comet morphology: the crystals start from an initial seed particle that grows within the droplet. When the crystal is first ejected, there is a drop in the contact angle to accommodate the large interface required to push out the initial seed crystal. As the precursor droplet is depleted, the growth transitions to a narrowing "tail". The shape of the tail is affected by variation in the growth angle; both linear and concavity switching morphologies are seen experimentally and are explained by the geometric model. The shape of the head can be significantly altered by deformation in the precursor droplet by varying the balance of ejection rate to crystallization rate.

The tailed distributions in the 2.00 wt % histogram in Figure 5B can be understood using the geometric model. We noted that the height of the crystal is proportional to  $\phi_{\rm g}$ . The height can be increased further by allowing  $\phi_{\rm g}$  to increase. In fact, there is a nonlinear relationship between the crystal height and the initial growth angle as can be seen in Figure 8. The gray

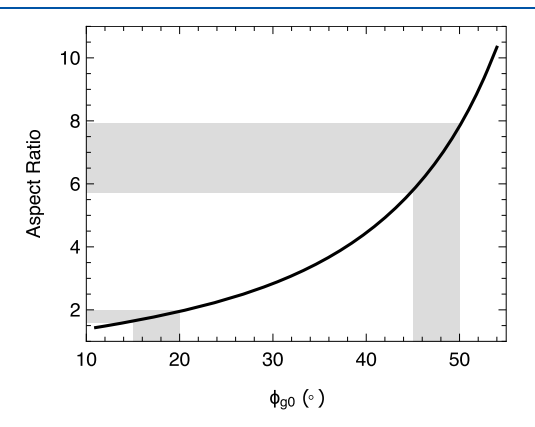


**Figure 8.** Aspect ratio of crystals as a function of their initial growth angle predicted using the geometric model. These measurements were made using the parameters  $\phi_0 = 175^\circ$ ,  $\phi_{\rm g}' = 0^\circ$ ,  $\rho = 1.0$ , and a fixed initial volume.

bands indicate the variation in aspect ratio due to a 5° change in  $\phi_{\rm g0}$ . At low  $\phi_{\rm g0}$ , this band is strongly attenuated, while high  $\phi_{\rm g0}$  results in a wider range of aspect ratios. A variation of just a few degrees can result in substantially longer crystals and create the tailed distribution that we observe experimentally. It is important to note that while  $\phi_{\rm g}$  might be a useful metric, the variability that we see is due to the stochastic nature of crystallization and complex flows of surfactants on the droplets not directly accounted for in the model.

To test the assumptions of the geometric model, we can a posteriori estimate the growth angle as a function of height by solving eq 4 for  $\phi_g$ . The results are shown in Figure 9 for the experimental crystals in Figure 7. The initial phases of growth show the most noise due to the difficulty of defining a contact

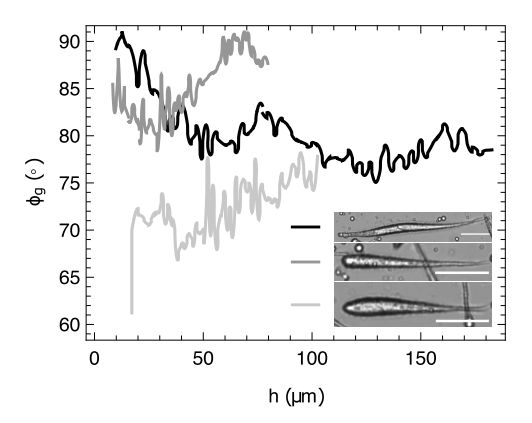


**Figure 9.** Growth angle as a function of height computed for experimental crystals. Scale bars are 50  $\mu$ m.

angle with little to no interface. While the relationship is more complicated than our linear assumption, we see good agreement with the trends seen in the geometric model. The crystal associated with the light gray curve shows a change in concavity. This implies that its growth angle should be increasing. We can estimate the initial growth angle to be somewhere between 50 and 70°. From the phase diagram in Figure 4, this is comfortably within the range of expected morphologies. The dark gray curve shows an overall increase in the growth angle. We would expect this, given its uniform tapering. The black curve has a high initial growth angle; as a result, we would expect the crystal to be very thin. This crystal then widens, which leads to a decrease in growth angle. The peak appears to be associated with the midpoint of this crystal, where it begins to grow smaller again. In all cases, the maximum growth angle stays below the upper limit of 90°.

As with other dynamic wetting processes, <sup>26,27,28</sup> the precursor droplet does not generally adopt the Young—Dupré contact angle set by the interfacial tensions in the system. If the oil droplet is distorted such that it forms a spherical cap with a smaller contact angle due to viscous drag, we would expect it to be proportional to velocity. Greater distortion of the oil droplet is seen when crystallization is dominant. From previous work, we know that the droplet velocity scales with the crystallization rate. <sup>11</sup> This might suggest that the force on the droplet is greater, causing the droplet to deform and shift the contact angle.

While the crystals observed here are three-dimensional, because the reaction occurs in bulk fluid, the presence of interfaces can cause flattened crystals to grow. We occasionally observe this experimentally where the initial precursor droplet rests on the glass substrate. In the Supporting Information, we display the results of an analogous calculation to that performed above, where eqs 2 and 3 are modified for two-dimensional (2D) space. While the trends observed are similar to those for axisymmetric three-dimensional (3D) droplets, the use of interfaces to control the sculpting process is an interesting avenue for future work.

#### CONCLUSIONS

In this work, we have constructed and tested a model to predict the range of accessible morphologies for a dewettingcontrolled sculpting process to produce anisotropic particles, comets, from spherical droplets, and their dependence on material parameters. We find that the most dramatic influence on the resulting shape comes from the growth direction of the crystallization, which is distinct from the precursor—back-ground interface and varies dynamically. Experimentally observed shapes are consistent with a linear dependence of growth angle on position, despite the more complicated relationship suggested by Figure 9.

The scenario considered here is interesting because while the complex shapes are sculpted by a hydrodynamic process, the length scale is small enough that an analytical description is possible using some geometric assumptions. Fluid flows and thermal stresses may influence the resulting shapes, but their effects are too rapid to be resolved on this time scale. The nonuniformity of the crystals seen experimentally does suggest, however, that there is a degree of stochasticity not captured in the geometric model developed here that deserves further study. Understanding the role of kinetics and the cooling rate in the sculpting process is an important target for future work. The geometric model developed can be readily adapted to other growth conditions and geometries and hence provides a useful vehicle for the prediction and design of complex shape formation from simple starting materials. Complex colloid shape design has applications in disparate areas like drug delivery, active matter, and large-scale self-assembly. Because of the wide range of shapes possible in even simple systems, it is critical that a viable feedback loop be developed between the design, synthesis, and testing of particle shape performance. Simple models, like ours, that provide efficient computational performance and prediction of complex shapes from experimental parameters will be essential to develop and use new materials.

#### ASSOCIATED CONTENT

### **5** Supporting Information

The Supporting Information is available free of charge at https://pubs.acs.org/doi/10.1021/acs.langmuir.0c02249.

Information about the initial emulsion droplet distributions and details on the 2D geometric model (PDF)

# AUTHOR INFORMATION

#### **Corresponding Author**

Timothy J. Atherton — Department of Physics and Astronomy, Tufts University, Medford, Massachusetts 02155, United States; Email: Timothy.Atherton@tufts.edu

#### **Authors**

Mathew Q. Giso — Department of Physics and Astronomy, Tufts University, Medford, Massachusetts 02155, United States; © orcid.org/0000-0003-2724-514X

Haoda Zhao – School of Chemical Engineering, University of New South Wales, Kensington, New South Wales 2033, Australia

Patrick T. Spicer — School of Chemical Engineering, University of New South Wales, Kensington, New South Wales 2033, Australia; orcid.org/0000-0002-8562-3906

Complete contact information is available at: https://pubs.acs.org/10.1021/acs.langmuir.0c02249

#### Notes

The authors declare no competing financial interest.

## ACKNOWLEDGMENTS

This material is based upon work supported by the National Science Foundation under Grant DMR-1654283. The authors

also acknowledge partial support from the Australian Government through the Australian Research Council's Discovery Projects funding scheme, Project DP150100865.

#### REFERENCES

- (1) Kralova, I.; Sjöblom, J. Surfactants used in food industry: a review. J. Dispersion Sci. Technol. 2009, 30, 1363–1383.
- (2) Lam, R. S.; Nickerson, M. T. Food proteins: a review on their emulsifying properties using a structure—function approach. *Food Chem.* **2013**, *141*, 975–984.
- (3) Velev, O. D.; Lenhoff, A. M.; Kaler, E. W. A class of microstructured particles through colloidal crystallization. *Science* **2000**, 287, 2240–2243.
- (4) Kedar, U.; Phutane, P.; Shidhaye, S.; Kadam, V. Advances in polymeric micelles for drug delivery and tumor targeting. *Nanomed.: Nanotechnol., Biol. Med.* **2010**, *6*, 714–729.
- (5) Cholakova, D.; Valkova, Z.; Tcholakova, S.; Denkov, N.; Smoukov, S. K. "Self-Shaping" of Multicomponent Drops. *Langmuir* **2017**, *33*, 5696–5706.
- (6) Fredrick, E.; Walstra, P.; Dewettinck, K. Factors governing partial coalescence in oil-in-water emulsions. *Adv. Colloid Interface Sci.* **2010**, *153*, 30–42.
- (7) McClements, D. J. Crystals and crystallization in oil-in-water emulsions: Implications for emulsion-based delivery systems. *Adv. Colloid Interface Sci.* **2012**, *174*, 1–30.
- (8) Boode, K.; Walstra, P. Partial coalescence in oil-in-water emulsions 1. Nature of the aggregation. *Colloids Surf., A* **1993**, *81*, 121–137.
- (9) Boode, K.; Walstra, P.; de Groot-Mostert, A. Partial coalescence in oil-in-water emulsions 2. Influence of the properties of the fat. *Colloids Surf., A* **1993**, *81*, 139–151.
- (10) Rousseau, D. Fat crystals and emulsion stability-a review. *Food Res. Int.* **2000**, 33, 3–14.
- (11) Spicer, P. T.; Hartel, R. W. Crystal comets: Dewetting during emulsion droplet crystallization. *Aust. J. Chem.* **2005**, *58*, 655–659.
- (12) Malmsten, M.; Lindman, B. Ellipsometry studies of cleaning of hard surfaces. Relation to the spontaneous curvature of the surfactant monolayer. *Langmuir* **1989**, *5*, 1105–1111.
- (13) Baeckstroem, K.; Lindman, B.; Engstroem, S. Removal of triglycerides from polymer surfaces in relation to surfactant packing. Ellipsometry studies. *Langmuir* **1988**, *4*, 872–878.
- (14) Schroeder, A.; Levins, C. G.; Cortez, C.; Langer, R.; Anderson, D. G. Lipid-based nanotherapeutics for siRNA delivery. *J. Intern. Med.* **2010**, 267, 9–21.
- (15) Kaialy, W.; Alhalaweh, A.; Velaga, S. P.; Nokhodchi, A. Effect of carrier particle shape on dry powder inhaler performance. *Int. J. Pharm.* **2011**, *421*, 12–23.
- (16) Gilbertson, K.; Finlay, W.; Lange, C.; Brett, M.; Vick, D. In Nanofabrication of High Aspect Ratio Aerosol Particles for Deposition Studies in a Model Human Airway, International Conference on MEMS, NANO and Smart Systems (ICMENS'04); 2004; pp 268–270.
- (17) Hartel, R. W. Crystallization in Foods; Aspen Publishers, 2001.
- (18) Méndez-Velasco, C.; Goff, H. D. Fat structure in ice cream: A study on the types of fat interactions. *Food Hydrocolloids* **2012**, 29, 152–159
- (19) Donev, A.; Cisse, I.; Sachs, D.; Variano, E. A.; Stillinger, F. H.; Connelly, R.; Torquato, S.; Chaikin, P. M. Improving the density of jammed disordered packings using ellipsoids. *Science* **2004**, *303*, 990–993.
- (20) Anderson, D.; Worster, M. G.; Davis, S. H. The case for a dynamic contact angle in containerless solidification. *J. Cryst. Growth* **1996**, *163*, 329–338.
- (21) Sanz, A. The crystallization of a molten sphere. *J. Cryst. Growth* **1986**, 74, 642–655.
- (22) Sanz, A.; Meseguer, J.; Mayo, L. The influence of gravity on the solidification of a drop. *J. Cryst. Growth* 1987, 82, 81–88.

- (23) Virozub, A.; Rasin, I. G.; Brandon, S. Revisiting the constant growth angle: Estimation and verification via rigorous thermal modeling. *J. Cryst. Growth* **2008**, *310*, 5416–5422.
- (24) Fisher, G.; Seacrist, M. R.; Standley, R. W. Silicon crystal growth and wafer technologies. *Proc. IEEE* **2012**, *100*, 1454–1474.
- (25) Ergun, R.; Hartel, R. W.; Spicer, P. T. Kinetic effects on interfacial partitioning of fat crystals. *Food Struct.* **2015**, *5*, 1–9.
- (26) De Gennes, P.-G. Wetting: statics and dynamics. Rev. Mod. Phys. 1985, 57, No. 827.
- (27) Gao, L.; McCarthy, T. J. Contact angle hysteresis explained. *Langmuir* **2006**, *22*, 6234–6237.
- (28) Bonn, D.; Eggers, J.; Indekeu, J.; Meunier, J.; Rolley, E. Wetting and spreading. *Rev. Mod. Phys.* **2009**, *81*, No. 739.
- (29) Schneider, C. A.; Rasband, W. S.; Eliceiri, K. W. NIH Image to Image]: 25 years of image analysis. *Nat. Methods* **2012**, *9*, 671.
- (30) Williams, D. L.; Kuhn, A. T.; Amann, M. A.; Hausinger, M. B.; Konarik, M. M.; Nesselrode, E. I. Computerised measurement of contact angles. *Galvanotechnik* **2010**, *101*, 2502.
- (31) Lamour, G.; Hamraoui, A.; Buvailo, A.; Xing, Y.; Keuleyan, S.; Prakash, V.; Eftekhari-Bafrooei, A.; Borguet, E. Contact angle measurements using a simplified experimental setup. *J. Chem. Educ.* **2010**, *87*, 1403–1407.
- (32) Schindelin, J.; Arganda-Carreras, I.; Frise, E.; Kaynig, V.; Longair, M.; Pietzsch, T.; Preibisch, S.; Rueden, C.; Saalfeld, S.; Schmid, B.; et al. Fiji: an open-source platform for biological-image analysis. *Nat. Methods* **2012**, *9*, 676.
- (33) Jin, C.; Krüger, C.; Maass, C. C. Chemotaxis and autochemotaxis of self-propelling droplet swimmers. *Proc. Natl. Acad. Sci. U.S.A.* **2017**, *114*, 5089–5094.
- (34) Quéré, D. Fluid coating on a fiber. *Annu. Rev. Fluid Mech.* **1999**, 31, 347–384.